Mechanical Properties of the Lateral Cortex of Mammalian Auditory Outer Hair Cells

J. A. Tolomeo,* C. R. Steele,# and M. C. Holley*
*Department of Physiology, University of Bristol, Bristol BS8 1TD England, and #Division of Applied Mechanics, Stanford University, Stanford, California 94305 USA

ABSTRACT Mammalian auditory outer hair cells generate high-frequency mechanical forces that enhance sound-induced displacements of the basilar membrane within the inner ear. It has been proposed that the resulting cell deformation is directed along the longitudinal axis of the cell by the cortical cytoskeleton. We have tested this proposal by making direct mechanical measurements on outer hair cells. The resultant stiffness modulus along the axis of whole dissociated cells was 3×10^{-3} N/m, consistent with previously published values. The resultant axial and circumferential stiffness moduli for the cortical lattice were 5×10^{-4} N/m and 3×10^{-3} N/m, respectively. Thus the cortical lattice is a highly orthotropic structure. Its axial stiffness is small compared with that of the intact cell, but its circumferential stiffness is within the same order of magnitude. These measurements support the theory that the cortical cytoskeleton directs electrically driven length changes along the longitudinal axis of the cell. The Young's modulus of the circumferential filamentous components of the lattice were calculated to be 1×10^7 N/m^2. The axial cross-links, believed to be a form of spectrin, were calculated to have a Young's modulus of 3×10^6 N/m^2. Based on the measured values for the lattice and intact cell cortex, an estimate for the resultant stiffness modulus of the plasma membrane was estimated to be on the order of 10^{-3} N/m. Thus, the plasma membrane appears to be relatively stiff and may be the dominant contributor to the axial stiffness of the intact cell.

INTRODUCTION

Outer hair cells are thought to improve the frequency response and sensitivity of the mammalian ear by generating high-frequency cell length changes that sharpen the amplitude and tuning of basilar membrane motion (Johnstone et al., 1986; Ruggero and Rich, 1991; Nuttall and Dolan, 1993; Mammano and Ashmore, 1993). The length changes can occur at frequencies of over 40 kHz in vitro (Xue et al., 1993), and the maximum deformation, expressed at low frequencies, is about 5% of cell length (Ashmore, 1987; Holley and Ashmore, 1988a; Dallos et al., 1991). The motility is directly dependent upon the electrical potential across the plasma membrane (Ashmore, 1987; Santos-Sacchi and Dilger, 1988; Dallos et al., 1991) and is particularly interesting because it provides large voltage-displacement relationships that are much greater than those of common engineering piezoelectric crystals (Tolomeo and Steele, 1995).

The present evidence indicates that the biophysical mechanism that drives the length changes is distributed along the lateral cortex and is not directly dependent on chemical intermediates such as calcium and ATP (Kachar et al., 1986; Holley and Ashmore, 1988a; Dallos et al., 1991; Kalinec et al., 1992; Huang and Santos-Sacchi, 1993). The voltage sensor and the motor elements for electromechanical transduction lie within the lateral plasma membrane (Kalinec et al., 1992; Huang and Santos-Sacchi, 1993), which supports an unusually high density of membrane protein (Gulley and Reese, 1977; Forge, 1991; Kalinec et al., 1992). Functionally, the stiffness of the plasma membrane must be at least within the same order as that of the rest of the cell cortex, otherwise it could not efficiently influence cell length. To drive cell length changes, the forces generated within the plane of the plasma membrane are expressed primarily along the longitudinal axis, even when the constraint of internal fluid is removed (Dallos et al., 1993). However, there is no structural evidence that this directionality is a function of the membrane or its integral proteins (Gulley and Reese, 1977; Forge, 1991; Kalinec et al., 1992).

Directionality could be provided by the cortical cytoskeletal lattice, a specialized cytoskeleton that lines the inner surface of the plasma membrane (Bannister et al., 1988; Holley and Ashmore, 1988b; Arima et al., 1991; Holley et al., 1992). The cortical lattice is composed of parallel filaments about 5–7 nm thick and 50–80 nm apart, that are wound circumferentially about the cell and cross-linked at intervals of 12–25 nm by thinner filaments about 2–3 nm thick (Holley and Ashmore, 1990; Holley et al., 1992). Circumferential filaments are connected to the plasma membrane by protein pegs about 30 nm long and spaced about 30 nm apart (Saito, 1983; Flock et al., 1986). Morphological and immunological studies suggest that circumferential filaments are composed largely of polymeric actin and that the cross-links are composed of a form of spectrin (Holley and Ashmore, 1990; Holley et al., 1992; Nishida et al., 1993). Spectrin molecules are compliant and elastic (Vertessy and Steck, 1989; McGough and Josephs, 1990), whereas actin is expected to have greater stiffness (Gittes et al., 1993; Kojima et al., 1994). Consequently, the cortical

Received for publication 19 September 1995 and in final form 15 April 1996.

Address reprint requests to Dr. Matthew C. Holley, Department of Physiology, Medical Sciences, University Walk, Bristol BS8 1TD, England. Tel.: 117-9287811; Fax: 117-9288923; E-mail: m.c.holley@bristol.ac.uk.

0006-3495/96/07/421/09 $2.00

lattice may be much stiffer circumferentially than it is longitudinally, thus directing forces generated within the plasma membrane into deformation along the cell axis.

In this study, the individual structural layers of the cell cortex are correlated with measured mechanical properties of the cell on the assumption that the mechanical properties of each layer (Fig. 1) contribute to the stiffness of the entire cell cortex (Steele, 1990). The main aim was to test the idea that the cortical lattice is an orthotropic structure in which the longitudinal stiffness is significantly less than the circumferential stiffness (Holley and Ashmore, 1988a). This should provide evidence of whether the lattice can provide the orthotropic properties and directionality characteristic of the intact cell (Dallos et al., 1993; Tolomeo and Steele, 1995) and should allow estimates to be made of the mechanical properties of its individual protein filaments. The second aim was to estimate the mechanical properties of the cell membranes by comparing measurements from whole cells with similar measurements from the cortical lattice alone. The results should provide some insight into how biological systems utilize materials to achieve specific mechanical requirements.

MATERIALS AND METHODS

Cell preparation

Guinea pigs were killed by cervical dislocation and their cochleae removed. The organs of Corti were dissected from the cochlea in Liebovitz L-15 (Gibco) solution and cells were dissociated by rapidly cycling the organ of Corti repeatedly through a pipette tip. The dissociated cells were then mounted on a protein-coated glass slide containing a well of about 400 μl of L-15 solution. The protein coat, designed to prevent the cells from adhering to the slide, was applied by incubating slides with 10% fetal calf serum for 20 min at 37°C. Slides were then rinsed in L-15 before use. All cell measurements were taken within 3 h of removal from the animal.

Cells were viewed through a Nikon Diaphot inverted microscope. Video images were processed with an image enhancer (Brian Reece Scientific) and recorded in real time with a JVC TK-1280E video camera, JVC super VHS recorder, and JVC TM-1500PS monitor. Quantitative analysis was performed by replaying the video through the image enhancer to imaging analysis software (Brian Reece Scientific).

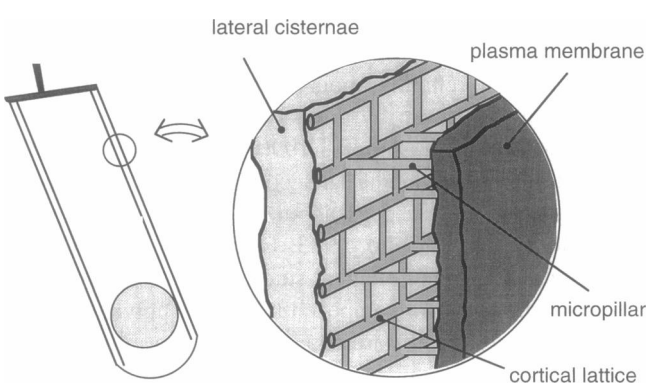

FIGURE 1 Sketch of cortical layers as described by Holley and Ashmore (1990). The lateral cisternae are located interior to the cortical lattice and have been drawn as one layer for clarity. The actual number of cisternal membrane layers is variable.

Construction and calibration of probes

Three different kinds of probes were used. Static probes for three-point bending measurements were made from glass micropipettes (Clark Electromedical F120) that had been pulled and bent at 90° near the tip. They were rigid probes of relatively short length with large tip diameters of about 5 μm, which tapered very quickly to about 50 μm. Measurement probes were made from the same glass pulled against a hot wire to form a long extended tip about 1 μm in diameter. The tip was then cut to a length of approximately 0.5 mm. Calibration probes were made from individual fibers of glass wool of about 13 μm in diameter and 10 mm long with very uniform diameter and cross section along the fiber length. They were bonded to the ends of glass micropipettes.

The stiffness of the measurement probes could not be measured directly with good accuracy because they were so small and compliant. The stiffness of the calibration probe was measured directly through a horizontal microscope at ×400 magnification by applying a 240-μg mass at different points along its length (Fig. 2). The mass was large enough to measure directly, thus avoiding errors introduced by estimating volume and density. The force-displacement results showed a definite cubic dependence on length, as predicted from beam bending theory. The close agreement with theoretical behavior allowed the extrapolation of results to the probe end where the stiffness was too small to measure directly.

The calibrated probe was then used to measure the stiffness of the smaller measurement probe by pressing the two probe tips together and measuring the relative displacement of each. The displacement ratio was inversely proportional to the stiffness ratio. The orientation of each probe was recorded and reproduced throughout each experiment to eliminate the possible effects of a nonsymmetric probe cross section. Measurement probes were completely submerged in the saline bath during the experiment.

All measurements of probe stiffness and dimensions were repeated between 10 and 20 times, so that random error could be assessed. Measurements of cell displacement were taken only twice, so the error used on these measurements was the resolution of the imaging software. Errors in the cell stiffness thus arose from the probe stiffness errors and cell displacement resolution error. The largest mechanical contributor was the probe stiffness error, which was generally about 10% of the probe stiffness value. The resolution of the imaging system conservatively gave measurement repeatability of ± 0.3 μm.

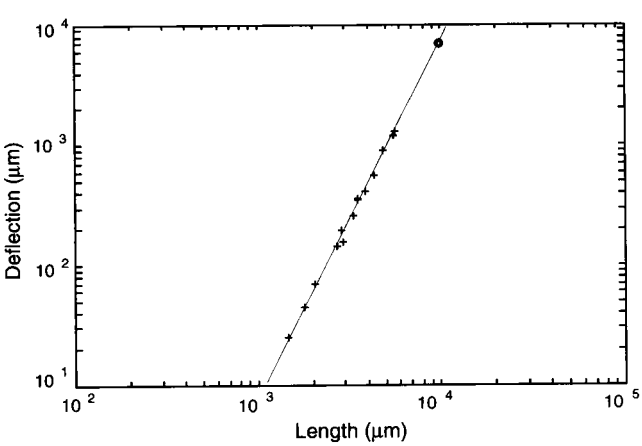

FIGURE 2 Stiffness of calibration probe. A known mass was placed along the length of a long glass fiber, and the deflection was measured. Results show excellent agreement with a theoretically predicted cubic dependence on length. Data were then extrapolated to the probe tip, where the stiffness was too small to be measured directly with good accuracy. +, measured values; −, cubic curve fit; ○, extrapolated value at probe tip.

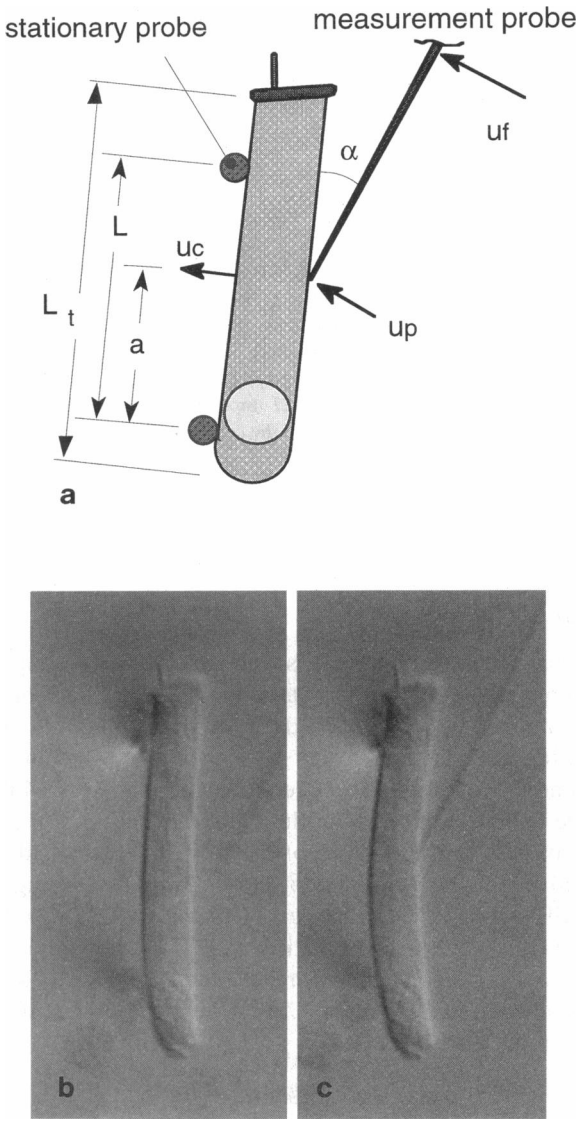

FIGURE 3 (*a*) Geometry and nomenclature used in the three-point bend test as defined in the text. Stationary probes were bent micropipettes. The measurement probe was driven at approximately 1 Hz. (*b*) A differential interference contrast image of a single outer hair cell with stationary and measurement probes arranged as in *a*. The cell diameter is 10 μm. (*c*) As in *b* but with the measurement probe deflecting the cell by about 2 μm at the point of application.

Three-point bending measurements

In the three-point bending test the two static probes were placed against each end of one side of the cell. The measurement probe was applied to the opposite side midway between them (Fig. 3). The measurement probe was driven by a piezoelectric bender element connected to a feedback FG601 signal generator at about 1 Hz and 6 μm maximum free displacement. The difference in the probe displacement under free conditions and when in contact with the cell gave the force at the probe tip and, therefore, the force on the cell. Maximum axial strains induced in the cell were about 3%.

Application of beam theory to the three-point bending measurements assumes that the stress distribution is constant through the thin cell cortex and the stress is linear in distance along the circumference of the cell in the direction of the applied load. In practice, the probe often produced a dimple in the cell cortex to a depth of about 1 μm and total width of about 2 μm.

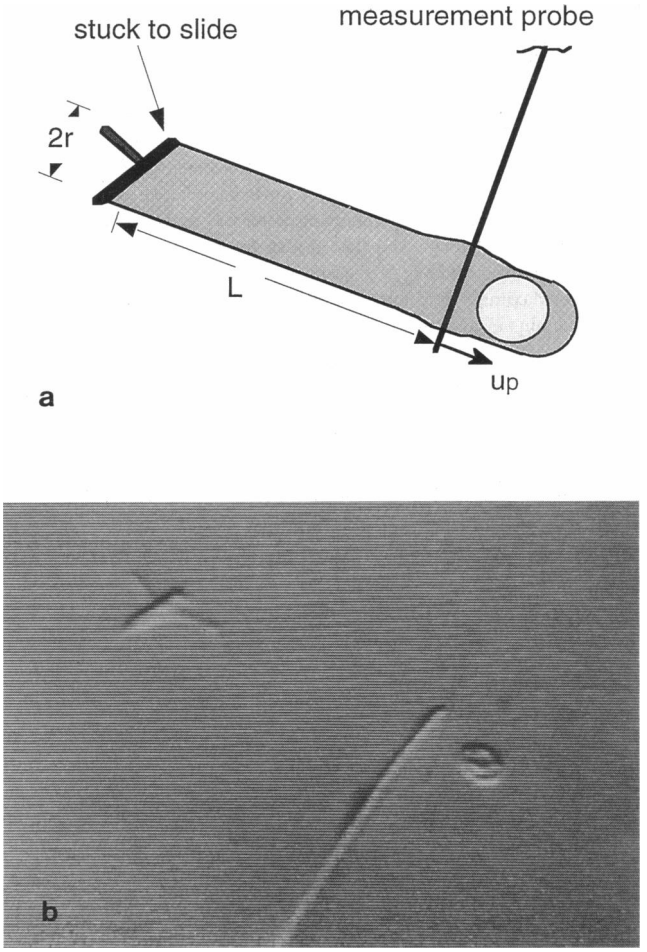

FIGURE 4 (*a*) Geometry for the axial measurements of cortical lattice. The measurement probe was placed beneath the cell before the addition of 0.1% Triton solution. After the membranes were dissolved, the cell ghost was gently lifted to prevent friction effects with the glass slide. The apical portion of the cell remained stationary and adhered to the slide. (*b*) The micrograph shows a detergent extracted cell being attached to the measurement probe. The larger probe was briefly used to stick the cell to the measurement probe.

This local deformation was highly elastic and followed the probe motion. It represented a true localized material bending phenomenon, intimately associated with the relative stiffness and spatial position of each structural layer of the cortex as well as the magnitude of the internal fluid pressure. Such a local deformation would have a small effect on the global beam bending stress and deformation, which exist throughout the entire length of the cell. However, to further minimize this local effect, cell displacements were measured from the side opposite the probe, whereas the applied force calculations were made based on the probe displacement. Although the dimpling was not utilized in the measurements directly, it was a useful indicator of cell condition, because large or inelastic deformations would be expected in deteriorating cells that had insufficient turgor pressure.

Cell condition was assessed visually and mechanically. Healthy cells were of uniform radius with the nucleus located basally. A probe was used to ensure that they were neither flaccid nor stuck to the slide before measurement.

Measurements from the cortical cytoskeleton

Measurements of the cytoskeletal lattice were made from cells whose membranes were extracted with 0.1% Triton X-100 in a solution of L-15

with a cocktail of enzyme inhibitors (100 μg/ml phenylmethylsulfonylfluoride, 1 μg/ml pepstatin, 1 μg/ml leupeptin, and 2 mM benzamidine). These inhibitors were not present in all experiments. Measurements of the longitudinal stiffness of the cytoskeletal lattice were made from cells stuck at their cuticular plates to the surface of a slide that was not coated with protein (Fig. 4). A measurement probe was positioned beneath the cell before the membranes were extracted. An additional probe was applied briefly to ensure that the extracted cytoskeletal lattice adhered to the measurement probe. The measurement probe was pretensioned by adjusting the micromanipulator and then driven by the piezoelectric bimorph. The relative displacements of the apical and basal ends of the cell were recorded. Maximum prestrain was about 10%, and the oscillating load induced strains of about 3%.

For circumferential stiffness measurements of the lattice, the cells were dissociated more vigorously to remove their cuticular plates. Both static and measurement probes were then inserted into the cell and pretensioned across it by adjusting the micromanipulators (Fig. 5). In most cases the probes penetrated the cell to a depth of about 20 μm. Displacement of the measurement probe was initiated once the probes were located, and the cell membranes were subsequently extracted with 0.1% Triton X-100. Maximum circumferential strains were about 10%, with an additional 10% prestrain. Cell condition was assessed as above. For circumferential measurements of the cytoskeletal lattice, only cells that retained a uniform cylindrical body were used.

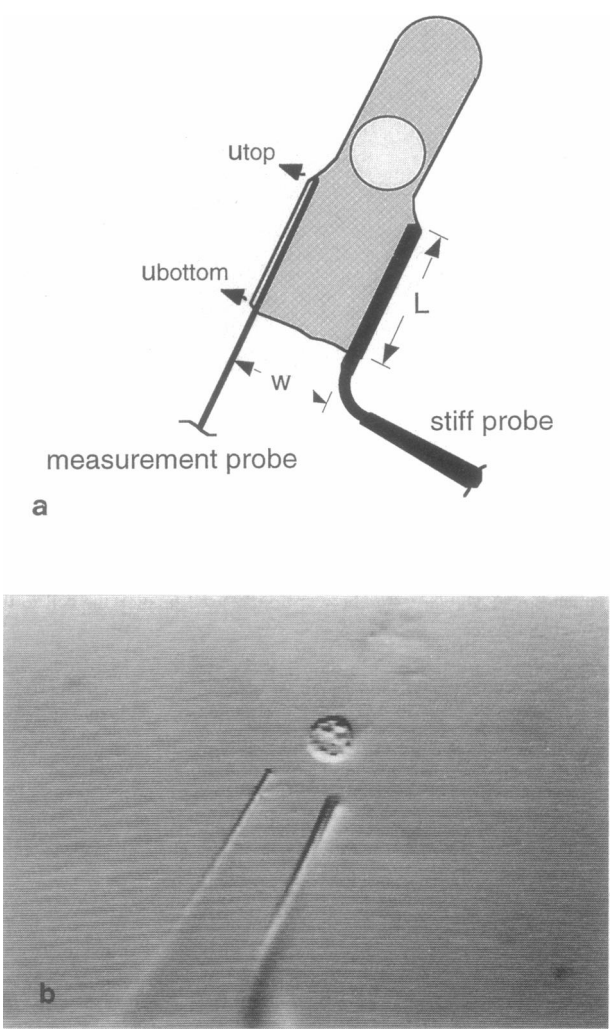

FIGURE 5 (*a*) Geometry for the circumferential measurements of the cortical lattice. The probes were placed within the decapitated cell before the addition of the 0.1% Triton solution. After the membranes were dissolved, the cell was lifted off the glass slide and slightly prestrained so that subsequent measurements were in the tension regime. (*b*) The micrograph shows the probes inserted into the cell and stretching the lattice. The outline of the cortical skeleton is barely visible between the probes.

Error analysis

The analysis presented here uses small strain elasticity within the formalism of continuum mechanics. Measurements were made under quasistatic conditions, so that viscosity and inertial effects were neglected. Throughout the analysis, systematic and random error propagation was tracked and reported. At least two types of error were present in the experiment. The first was a result of the mechanical methods and measurements employed. These could be estimated and tracked throughout the calculations. The second was the health and condition of the cells as compared to the in vivo state. This could not be quantified and therefore no estimate is given, but it is likely to be the largest source of variation in the results.

RESULTS

Axial cortex modulus

The three-point bending test is well suited to measuring the axial modulus of the cell, because the opposing sides of the cell are theoretically strained by opposite amounts. The resulting deformation occurs with no net change in cell volume or Poisson effect. Therefore, the incompressibility of the internal fluid and the fluid pressure are not affected. The axial stiffness modulus of the cell cortex is calculated directly from one measurement and is a weighted average of the stiffness of all the structural layers within the cortex. For convenience, the structural stiffness k_{cell} is defined as the ratio of the perpendicular force F at the cell wall to the perpendicular displacement u_c at the cell wall. The stiffness relation is given by

$$k_{cell} \equiv \frac{F}{u_c} = \frac{k_p (u_f - u_p)}{u_c \cos \alpha}, \tag{1}$$

where k_p is the measurement probe stiffness, u_f is the measurement of the free probe displacement, u_p is the measurement probe displacement during contact, and α is the angle between the cell and the probe (Fig. 3). The quantity k_{cell} represents the structural stiffness of the cell, and it is highly dependent on the distance between the stationary probes. This value alone gives little insight into the material properties. However, it can be incorporated into a beam bending model that allows the axial resultant stiffness modulus Et_{cell} of the cell cortex to be determined. The resultant modulus is defined as the product of the Young's modulus and the material thickness. It is characteristic of the cell material and independent of the location of the probes or structural geometry other than thickness. For a long, thin-walled, cylindrical beam simply supported at both ends, the displacement at the load application site is given by Euler beam theory (Roarke, 1965):

$$u_c = \frac{F (L^2 a^2 - 2La^3 + a^4)}{3 \pi E t_{cell} r^3 L}. \tag{2}$$

The geometry is as defined in Fig. 3, where L is the length between probes, r is the cell radius, and a is the distance from the probe to the force contact site. Combining Eqs. 1 and 2 gives the axial resultant stiffness modulus

$$Et_{cell} = \frac{k_{cell}(L^2a^2 - 2La^3 + a^4)}{3\pi r^3 L}. \quad (3)$$

The mean axial modulus for 22 cells was measured to be $Et_{cell} = 3 \times 10^{-3} \pm 1 \times 10^{-3}$ N/m, where the error in the mean was taken as one standard deviation about the mean (Fig. 6). The error estimates for individual stiffness values were also calculated based on calibration error and subsequently used to determine the resolution of the data and possible length dependence in the material modulus. However, no correlation between stiffness modulus and cell length was identified within the limits of the experimental error.

Cortical lattice

Axial measurements of the extracted cortical lattice were made by applying longitudinal tension via the measurement probe. Tension measurements rather than compression were desired, to ensure that buckling of the lattice did not give erroneously compliant measurements. The applied load produced an essentially uniaxial stress state in which the deformation was modeled by the simple relation

$$E_x t = \frac{k_p(u_f - u_p)L}{2\pi r u_p}. \quad (4)$$

The geometry is shown in Fig. 4, where L is the length from the cell apex to the measurement probe, and r is the cell radius. The mean value of the resultant stiffness modulus for 20 cells was measured to be $E_x t = 5 \times 10^{-4} \pm 2 \times 10^{-4}$ N/m (Fig. 7). Prestrain ensured that the measurements were made in the tension regime. These stiffness measurements apparently were not affected by endogenous enzymes because they were independent of the presence of enzyme inhibitors and there was no systematic change throughout the duration of the experiment.

The circumferential stiffness of the cortical lattice was calculated in a manner similar to that of Eq. 4:

$$E_y t = \frac{k_p(u_f - u_{avg})w}{2L u_{avg}}. \quad (5)$$

The geometry is shown in Fig. 5, where w is the cell width when flattened and the term u_{avg} is the average of the measured displacement taken from the top and bottom contact points on the lattice. The mean stiffness modulus from 13 cells was measured to be $E_y t = 3 \times 10^{-3} \pm 2 \times 10^{-3}$ N/m (Fig. 7), where again the error on the mean was taken as one standard deviation about the mean. Error estimates on individual measurements were also plotted to indicate the resolution of the data.

These measurements of the lattice were made in the absence of turgor pressure and transcellular potential in contrast to the measurements of the axial cell cortex. When the cortex was permeabilized and the membrane layers dissolved away with the Triton solution, the cell was seen to increase in length by an average of about 6% taken over 19 cells. This indicates that in the turgid state, the cell exists in a state of negative prestrain. Because it was the purpose of this study to directly compare the stiffness of the lattice with the stiffness of the intact cortex, some estimate of the effect of prestrain on the material properties was necessary.

The effect of prestrain on the lattice stiffness measurements was estimated by measuring the change in stiffness of individual cells as the prestrain was increased. Fig. 8 shows the axial stiffness results from five cells tested. Some strain hardening is evident in the axial stiffness, although the

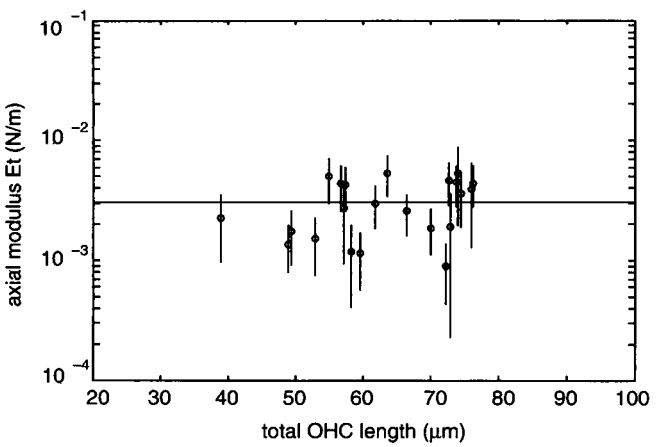

FIGURE 6 Axial stiffness modulus measured on the intact wall from cells of various lengths. Within the mechanical error estimates, the cell wall material modulus does not display a dependence on cell length. The average value from all data gives $Et_{cell} = 3 \times 10^{-3}$ N/m. O, experimental value with calibration error bars. The horizontal line is the average value from all data.

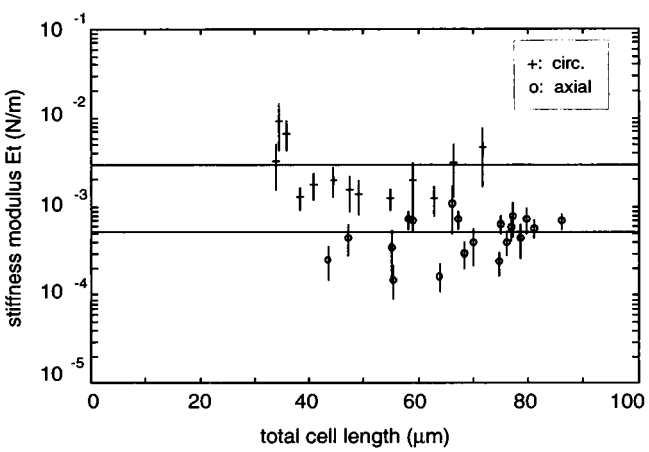

FIGURE 7 Resultant stiffness modulus for the cortical lattice. The circumferential direction is an order of magnitude stiffer than the axial direction. Thus the lattice is highly orthotropic, in agreement with morphological studies.

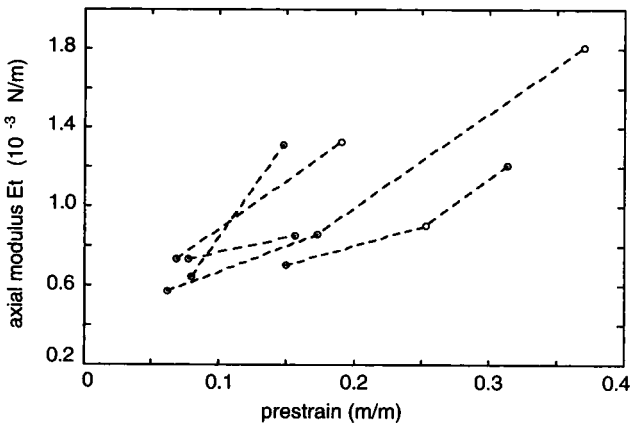

FIGURE 8 The effect of prestrain on the axial lattice stiffness. The stiffness of five cells was measured as the prestrain was increased. Some strain hardening is evident, although for strains less than 10%, the increase in stiffness is within the experimental scatter.

increase for prestrains less than 10% is on the order of experimental scatter. For this reason, all of the axial lattice results given in Fig. 7 were calculated from cells with prestrains of less than 10%. The circumferential stiffness measurements showed no dependence on prestrain. It is not possible to experimentally measure the effect of negative prestrain, because without the support of the plasma membrane the lattice is prone to buckling under compression. However, it is assumed that the effect of prestrain for small negative values of strain can be extrapolated from the results in Fig. 8. It is concluded that the small turgor negative prestrain produces a negligible change in the axial stiffness, and therefore the stiffness values measured here are good estimates of the lattice stiffness in the turgor state.

Plasma membrane

The resultant moduli calculated for the intact cell cortex and the cortical lattice can be used to calculate an upper bound on the mechanical properties of the other components of the cortex, particularly the lateral cisternae and plasma membrane. The membranes and cytoskeletal lattice can be modeled as the two layers that contribute additively to the stiffness of the intact cell. Therefore, by appropriately subtracting the stiffness of the lattice from the stiffness of the intact cell about the turgor state, it should be possible to gain an estimate of the stiffness of the membranes about the turgor state.

The problem of how each layer contributes to the total cell stiffness is rendered difficult by the two-dimensional anisotropy of the cell cortex. In general, the stiffness matrix of the intact cell is the sum of the stiffness of each component layer. The total stiffness matrix is then inverted to find the compliance matrix. The inverse of the diagonal terms in the compliance matrix is the resultant stiffness moduli (Nye, 1992). However, because the axial modulus of the cortical lattice was shown to be an order of magnitude smaller than the circumferential modulus and the intact cell modulus, this quantity can be neglected in the calculations. It is further assumed that the membranes are isotropic in the plane of the cortex. This gives a more simplified relation for the total cell axial modulus in terms of the moduli of the individual layers, which is accurate in the limit as $E_x t$ approaches zero.

$$Et_{\text{cell}} = \frac{Et_{\text{plasma}}\,(Et_{\text{plasma}} + E_y t)}{Et_{\text{plasma}} + E_y t(1 - \upsilon^2)}. \tag{6}$$

The Poisson ratio of the membrane (υ) plays a critical role in the behavior of the stiffness properties of the cortex. As the Poisson ratio goes to zero, such as in a simple one-dimensional analysis, Eq. 6 shows that the axial modulus of the membranes is equal to the axial modulus of the intact cell:

$$Et_{\text{plasma}} = Et_{\text{cell}} \quad \text{for } \upsilon = 0 \tag{7}$$

An upper bound on the resultant Young's modulus is given by Eq. 7. However, the Poisson ratio of the membranes is unlikely to be zero. Equation 8 was derived for the case where the Poisson ratio equals unity.

$$Et_{\text{plasma}} = Et_{\text{cell}} - Et_y \quad \text{for } \upsilon = 1 \tag{8}$$

This corresponds to areal incompressibility. Such a Poisson ratio is an idealization of a two-dimensional elastic incompressible medium and is unattainable in a physical material. However, based on the observations of the behavior of the intact cortex (Ashmore, 1987) and from the known properties of lipid bilayers, Eq. 8 is probably closer to the behavior of the lateral membranes. For example, the Poisson ratio for the red blood cell can be computed from calculations of areal and extensional moduli by Skalak et al. (1973) and Evans and Hochmuth (1978). This results in a red blood cell Poisson ratio of approximately 0.999. Applied to the outer hair cell, this would result in $Et_{\text{plasma}} = 1 \times 10^{-4}$ N/m. It is tempting to use this as a lower bound of the stiffness modulus, but a closer inspection of the error estimates of the measured stiffness moduli indicates that there is not sufficient resolution to make such a statement. It is concluded from this analysis that if the plasma membrane and lateral cisternae have a Poisson ratio of less than about 0.95 (Fig. 9), the resultant stiffness modulus is of the same order as the circumferential lattice stiffness modulus and the axial cell cortex stiffness modulus, that is $Et_{\text{plasma}} \approx 10^{-3}$ N/m.

DISCUSSION

Axial stiffness of outer hair cells

The mean axial stiffness modulus reported here of $Et_{\text{cell}} = 3 \times 10^{-3}$ N/m compares well with previously published values of total cell compliance that were based on uniaxial compression experiments. These total cell compliance measurements can be converted to a material property using the relation that the resultant Young's modulus is equal to the

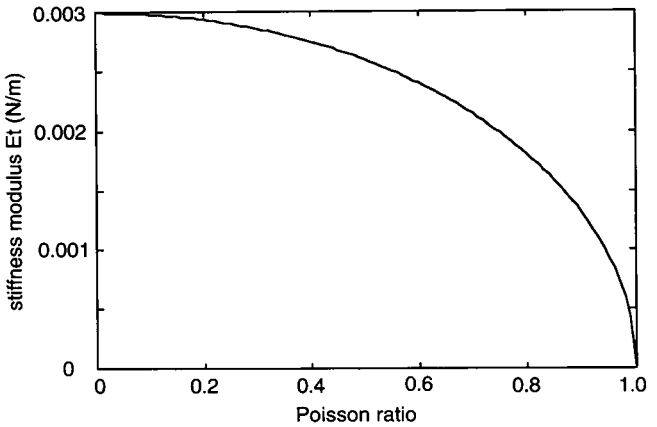

FIGURE 9 Effect of Poisson ratio on the calculation of the plasma membrane resultant stiffness modulus. The extreme range of Poisson values near unity represents areal incompressibility for a two-dimensional material, similar in behavior to a fluid. It is seen that for Poisson ratios less than about 0.95, the stiffness modulus of the plasma membrane is on the same order as the intact cell cortex stiffness modulus and the circumferential stiffness modulus of the lattice.

cell length divided by the product of the compliance and cell circumference. Our measured value of 3×10^{-3} N/m is very similar to values of 1×10^{-3} N/m and 6×10^{-3} N/m, which are derived from the compression experiments of Holley and Ashmore (1988b) and Hallworth (1995) respectively. The difference between the two experimental techniques is that compression should cause nearly constant stress throughout the cell, whereas the three-point bending deformation reported in this paper should be the result of stresses that vary linearly about the cell diameter. The good agreement between the two techniques supports our assumption that the material properties of the cell are homogeneous and continuous at the micrometer scale. Furthermore, within the limits of experimental error, there was no change in material stiffness with cell length, which implies that the material properties of outer hair cells remain constant throughout the cochlea.

The measured stiffness values also indirectly imply that turgor pressure may be less than has been previously reported. The above-referenced compression estimates for cell compliance are insensitive to turgor pressure as long as buckling is avoided, whereas the three-point bending experiment in our work would give artificially large stiffness values if the internal pressure were large. This is because pressure creates an internal tensile force that resists out-of-plane bending deformation but does not affect in-plane deformation. The effect of tension can cause significant modification of Eq. 2 for pressures on the order of 1 kPa. The good agreement with previous compliance measurements therefore indicates that turgor pressure is much less than 1 kPa. Ratnanather et al. (1993) estimated turgor pressure to be in the range of 0.17 to 1.9 kPa. Our stiffness values may be consistent with estimates of turgor pressures at the lower end of this range.

Orthotropic properties of the cortical lattice

The mean axial stiffness of $E_x t = 5 \times 10^{-4}$ N/m for the extracted cortical lattice was moderately greater than that of 1×10^{-4} N/m calculated from previous measurements (Holley and Ashmore, 1988b). As with the measurement of the intact-cell modulus, this is likely to be due to the difference between methods based upon tension and compression respectively. The results from both methods show that the axial stiffness of the cortical lattice is an order of magnitude less than that of the intact cell. However, the circumferential lattice stiffness, $E_y t = 3 \times 10^{-3}$ N/m, is very similar to the stiffness of the intact axial cell modulus. This result implies that it would be much easier to deform an outer hair cell axially than circumferentially.

Stiffness of circumferential filaments and cross-links

Because of the highly organized orthogonal structure of the cortical lattice, it is possible to use the lattice stiffness measurements to estimate the stiffness of its component protein filaments. A simple method for calculating the stiffness of the individual filaments is to multiply the lattice stiffness by the ratio of the filament spacing to the cross-sectional area of each type of filament. Assuming that circumferential and axial filaments are spaced at intervals of 60 nm and 25 nm, respectively, and that they are 5 nm and 2.5 nm in diameter (Holley et al., 1992), their Young's moduli are estimated to be about 1×10^7 N/m^2 and 3×10^6 N/m^2, respectively. A more detailed analysis that uses a tensor coordinate transformation to account for observed variations in the orientation of the filaments changes these stiffness values by at most a factor of 2 (Tolomeo, 1995). If the proposed protein composition of the cortical lattice is correct, then these Young's moduli should reflect those for actin polymers (circumferential filaments) and spectrin molecules (axial cross-links), respectively.

The stiffness of the circumferential filaments is much lower than recently published measurements from isolated actin filaments. Gittes et al. (1993) calculated a Young's modulus for actin of 3×10^9 N/m^2 based on a statistical model of thermal bending fluctuations, and Kojima et al. (1994) calculated a similar value of 2×10^9 N/m^2 based on extension of isolated actin filaments. Some of this difference may be explained by the effects of selected cations or actin-binding proteins, both of which are known to influence the stiffness of filamentous actin (Orlova and Egelman, 1993; Egelman and Orlova, 1995). Gittes et al. (1993) noted that their value for a single actin filament was much higher than that of nerve cell processes containing actin filaments, and their explanation was that the processes were not composed of continuous polymers and that the actin cross-linking proteins may be highly compliant. These arguments could also explain our relatively low values for the circumferential filaments that are not continuous around the cell

(Holley et al., 1992) and which may be linked by more compliant protein filaments.

In contrast, the dimensions of the axial cross-links strongly suggest that they are composed solely of some form of spectrin (Holley et al., 1992; Nishida et al., 1993). Although they do not form a continuous filament along the length of the lattice, each cross-link is firmly attached to a circumferential filament, thus effectively creating a continuous path for stress transfer. Our stiffness estimate for the cross-links (3×10^6 N/m^2) may represent a reasonable estimate for the Young's modulus of spectrin. The majority of published reports on the material properties of spectrin have been derived from the shear modulus of gels or have been made in conjunction with membranes such as the red blood cell (Nash and Gratzer, 1993). The mechanical properties are found to be highly shear compliant, but they cannot be directly related to filament extensional stiffness, because other mechanisms such as sliding and filament reorganization must be taken into account. Furthermore, the morphology of the red blood cell (Byers and Branton, 1985; Shen et al., 1986) shows a distribution of spectrin that does not possess the geometric regularity of the outer hair cell, so that the kind of microstructural interpretation possible with outer hair cells is less viable for the red blood cell. To our knowledge, the Young's modulus calculated here is the first direct measure of extensional stiffness of spectrin, and the value is similar to that of other rubbery proteins such as elastin and resilin (Wainwright et al., 1976).

Stiffness of the plasma membrane

The stiffness of the plasma membrane must be a significant component of the axial stiffness of the whole cell, assuming that it is the source of forces that drive high-frequency cell length changes. If it were not sufficiently stiff, most of the energy associated with conformal change would be stored in the plasma membrane itself as strain energy, whereas the rest of the stiffer cell cortex resisted the deformation. The structure of the plasma membrane in outer hair cells suggests that it is likely to be significantly stiffer than the cisternal membranes. The main difference is that it contains an extremely high density of membrane proteins, possibly as high as 6000/μm^2 (Gulley and Reese, 1977; Kalinec et al., 1992; Forge, 1991), a feature that should increase the stiffness more than any other single factor. Additional stiffness may come from the relatively high concentration of cholesterol, which allows closer packing of lipid molecules within the bilayer (Forge, 1991). The lateral cisternae contain few integral membrane proteins, as seen in preparations of freeze-fractured material (Gulley and Reese, 1977; Forge, 1991). Although there may be numerous membrane layers within the cisternae, the number varies from as many as nine to only two, both within and between cells, and they are often extensively fenestrated (Evans, 1990; Furness and Hackney, 1990; Forge et al., 1993). Our stiffness measurements show fairly uniform material properties throughout the length of individual cells and between both long and short cells, so we conclude that within the limits of our experimental error, the cisternal membranes contribute insignificantly to the material properties of the cortex. Therefore, the estimate of the resultant stiffness modulus of membrane layers given as $Et_{plasma} \approx 10^{-3}$ N/m can be considered as an estimate for the stiffness of the plasma membrane in the turgor state.

The plasma membrane may achieve stiffness in either of two ways. It may have a large Young's modulus, which would provide stiffness to any load condition, or it may have a large Poisson ratio (>0.95), which would impart large stiffness to areal changes corresponding to biaxial load conditions similar to those produced by internal pressure or electrical potential. The estimate of 10^{-3} N/m for the stiffness of the plasma membrane is much higher than that of the plasma membrane in red blood cells, which has been estimated to be 1×10^{-5} N/m (Skalak et al., 1973). Our estimated resultant stiffness modulus corresponds to moderate values of Poisson ratio associated with the plasma membrane. However, based on the resolution of the measurement techniques employed, it is not possible to calculate the Poisson ratio and give a better estimate of resultant stiffness. The plasma membrane has been proposed to effect motility through predominantly areal conformal change (Kalinec et al., 1992; Santos-Sacchi, 1993), in which case either mechanism would be effective.

We thank Prof. J. F. Ashmore and Dr. P. J. Kolston for helpful discussions.

This work was supported by The Wellcome Trust and a Royal Society Research Fellowship to MCH and U.S. Air Force grant AF 49620-92-J-0276 to CRS.

REFERENCES

Arima, T., A. Kuraoka, R. Toriya, Y. Shibata, and T. Uemura. 1991. Quick-freeze, deep-etch visualisation of the "cytoskeletal spring" of cochlear outer hair cells. *Cell Tissue Res.* 263:91–97.

Ashmore, J. F. 1987. A fast motile response in guinea pig outer hair cells: the cellular basis of the cochlear amplifier. *J. Physiol. (Lond.).* 388: 323–347.

Bannister, L. H., H. C. Dodson, A. F. Astbury, and E. E. Douek. 1988. The cortical lattice: a highly ordered system of subsurface filaments in guinea pig cochlear outer hair cells. *Prog. Brain Res.* 74:213–219.

Byers, T. J., and D. Branton. 1985. Visualisation of the protein associations in the erythrocyte membrane skeleton. *Proc. Natl. Acad. Sci. USA.* 82:6153–6157.

Dallos, P., B. N. Evans, and R. Hallworth. 1991. Nature of the motor element in electrokinetic shape changes of cochlear outer hair cells. *Nature.* 350:155–157.

Dallos, P., R. Hallworth, and B. N. Evans. 1993. Theory of electrically-driven shape changes of cochlear outer hair cells. *J. Neurophysiol.* 70:299–323.

Egelman, E. H., and A. Orlova. 1995. New insights into actin filament dynamics. *Curr. Opin. Struct. Biol.* 5:172–180.

Evans, B. N. 1990. Fatal contractions: ultrastructural and electromechanical changes in outer hair cells following transmembranous electrical stimulation. *Hear. Res.* 45:265–282.

Evans, E. A., and R. M. Hochmuth. 1978. Mechanochemical properties of membranes. *Curr. Top. Membr. Transport.* 10:1–64.

Flock, I., B. Flock, and M. Ulfendahl. 1986. Mechanisms of movement in outer hair cells and a possible structural basis. *Arch. Otorhinolaryngol.* 243:83–90.

Forge, A. 1991. Structural features of the lateral walls in mammalian cochlear outer hair cells. *Cell Tissue Res.* 265:473–483.

Forge, A., G. Zajic, L. Li, G. Nevill, and J. Schacht. 1993. Structural variability of the sub-surface cisternae in intact, isolated outer hair cells shown by fluorescent labelling of intracellular membranes and freeze-fracture. *Hear. Res.* 64:175–183.

Furness, D. N., and C. M. Hackney. 1990. Comparative ultrastructure of subsurface cisternae in inner and outer hair cells of the guinea pig cochlea. *Eur. Arch. Otorhinolaryngol.* 247:12–15.

Gittes, F., B. Mickey, J. Nettleton, and J. Howard. 1993. Flexural rigidity of microtubules and actin filaments measured from thermal fluctuations in shape. *J. Cell Biol.* 120:923–934.

Gulley, R. L., and T. S. Reese. 1977. Regional specialisation of the hair cell plasmalemma in the organ of Corti. *Anat. Rec.* 189:109–124.

Hallworth, R. 1995. Passive compliance and active force generation in the guinea pig outer hair cell. *J. Neurophysiol.* 74:2319–2328.

Holley, M. C., and J. F. Ashmore. 1988a. On the mechanism of a high-frequency force generator in outer hair cells isolated from the guinea pig cochlea. *Proc. R. Soc. Lond.* B232:413–429.

Holley, M. C., and J. F. Ashmore. 1988b. A cytoskeletal spring in cochlear outer hair cells. *Nature.* 335:635–637.

Holley, M. C., and J. F. Ashmore. 1990. Spectrin, actin and the structure of the cortical lattice in mammalian cochlear outer hair cells. *J. Cell Sci.* 96:283–291.

Holley, M. C., F. Kalinec, and B. Kachar. 1992. Structure of the cortical cytoskeleton in mammalian outer hair cells. *J. Cell Sci.* 102:569–580.

Huang, G., and J. Santos-Sacchi. 1993. Mapping the distribution of the outer hair cell motility voltage sensor by electrical amputation. *Biophys. J.* 65:2228–2236.

Johnstone, B. M., R. Patuzzi, and G. K. Yates. 1986. Basilar membrane measurements and the travelling wave. *Hear. Res.* 22:147–153.

Kachar, B., W. E. Brownell, R. Altschuler, and J. Fex. 1986. Electrokinetic shape changes of cochlear outer hair cells. *Nature.* 322:365–368.

Kalinec, F., M. C. Holley, K. Iwasa, D. J. Lim, and B. Kachar. 1992. A membrane-based force generation mechanism in auditory sensory cells. *Proc. Natl. Acad. Sci. USA.* 89:8671–8675.

Kojima, H., A. Ishijima, and T. Yanigida. 1994. Direct measurement of stiffness of single actin filaments with and without tropomyosin by in vitro nanomanipulation. *Proc. Natl. Acad. Sci. USA.* 91:12962–12966.

Mammano, F., and J. F. Ashmore. 1993. Reverse transduction measured in the isolated cochlea by laser Michelson interferometry. *Nature.* 365: 838–841.

McGough, A. M., and R. Josephs. 1990. On the structure of erythrocyte spectrin in partially expanded membrane skeletons. *Proc. Natl. Acad. Sci. USA.* 87:5208–5212.

Nash, G. B., and W. B. Gratzer. 1993. Structural determinants of the rigidity of the red cell membrane. *Biorheology.* 30:397–407.

Nishida, Y., T. Fujimoto, A. Takagi, I. Honjo, and K. Ogawa. 1993. Fodrin is a constituent of the cortical lattice in outer hair cells of the guinea pig cochlea: immunocytochemical evidence. *Hear. Res.* 65:274–280.

Nuttall, A. L., and D. F. Dolan. 1993. Basilar membrane velocity responses to acoustic and intracochlear electrical stimuli. *In* Biophysics of Hair Cell Sensory Systems. H. Duifuis, J. W. Horst, P. van Dijk, and S. M. van Netten, editors. World Scientific, Singapore. 288–295.

Nye, J. F. 1992. Physical Properties of Crystals. Oxford University Press, Oxford, England. 143.

Orlova, A., and E. H. Egelman. 1993. A conformational change in the actin sub-unit can change the flexibility of the actin filament. *J. Mol. Biol.* 232:1043–1053.

Ratnanather, J. T., W. E. Brownell, and A. S. Popel. 1993. Mechanical properties of the outer hair cell. *In* Biophysics of Hair Cell Sensory Systems. H. Duifuis, J. W. Horst, P. van Dijk, and S. M. van Netten, editors. World Scientific, Singapore. 199–206.

Roarke, R. J. 1965. Formulas for Stress and Strain, 4th Ed. McGraw-Hill, New York.

Ruggero, M. A., and N. C. Rich. 1991. Furosamide alters organ of Corti mechanics: evidence for feedback of outer hair cells upon the basilar membrane. *J. Neurosci.* 11:1057–1067.

Saito, K. 1983. Fine structure of the sensory epithelium of guinea pig organ of Corti: subsurface cisternae and lamellar bodies in the outer hair cells. *Cell Tissue Res.* 229:467–481.

Santos-Sacchi, J. 1993. Harmonics of outer hair cell motility. *Biophys. J.* 65:2217–2227.

Santos-Sacchi, J., and J. P. Dilger. 1988. Whole cell currents and mechanical responses of outer hair cells. *Hear. Res.* 35:143–150.

Shen, B. W., R. Josephs, and T. L. Steck. 1986. Ultrastructure of the intact skeleton of the human erythrocyte membrane. *J. Cell Biol.* 102: 997–1006.

Skalak, R., A. Torezen, R. A. Zarda, and S. Chien. 1973. Strain energy function of red blood cell membranes. *Biophys. J.* 13:245–264.

Steele, C. R. 1990. Elastic behavior of the outer hair cell wall. *In* Mechanics and Biophysics of Hearing. P. Dallos, C. D. Geisler, J. W. Matthews, M. A. Ruggero, and C. R. Steele, editors. Springer-Verlag. New York.

Tolomeo, J. A. 1995. Models of the structure and motility of the auditory outer hair cell. Ph.D. thesis. Stanford University, Stanford, CA.

Tolomeo, J. A., and C. R. Steele. 1995. Orthotropic piezoelectric properties of the cochlear outer hair cell wall. *J. Acoust. Soc. Am.* 97:3024–3029.

Vertessy, B. G., and T. L. Steck. 1989. Elasticity of the human red cell membrane skeleton. Effects of temperature and denaturants. *Biophys. J.* 55:255–262.

Wainwright, S. A., W. D. Biggs, J. D. Currey, and J. M. Gosline. 1976. Mechanical Design in Organisms. Princeton University Press, Princeton, NJ.

Xue, S., D. C. Mountain, and A. E. Hubbard. 1993. Direct measurement of electrically-evoked basilar membrane motion. *In* Biophysics of Hair Cell Sensory Systems. H. Duifuis, J. W. Horst, P. van Dijk, and S. M. van Netten, editors. World Scientific, Singapore. 361–369.